Eur. Phys. J. B **42**, 31–45 (2004)
DOI: 10.1140/epjb/e2004-00355-x

THE EUROPEAN PHYSICAL JOURNAL B

On the diffraction pattern of C_{60} peapods

J. Cambedouzou[1,a], V. Pichot[2], S. Rols[1], P. Launois[2], P. Petit[3], R. Klement[3,4], H. Kataura[5], and R. Almairac[1]

[1] Groupe de Dynamique des Phases Condensées (UMR CNRS 5581), Université Montpellier II, 34095 Montpellier Cedex 5, France
[2] Laboratoire de Physique des Solides (UMR CNRS 8502), Université Paris Sud, 91405 Orsay, France
[3] Institut Charles Sadron, 67000 Strasbourg, France
[4] Department of Physical Chemistry, Faculty of Chemical and Food Technology, Slovak Technical University, Radlinského 9, 812 32 Bratislava, Slovak Republic
[5] Nanotechnology Research Institute, National Institute of Advanced Industrial Science and Technology (AIST) Central 4, Higashi 1-1-1, Tsukuba, Ibaraki 305-8562, Japan

Received 19 May 2004
Published online 26 November 2004 –

Abstract. We present detailed calculations of the diffraction pattern of a powder of bundles of C_{60} peapods. The influence of all pertinent structural parameters of the bundles on the diffraction diagram is discussed, which should lead to a better interpretation of X-ray and neutron diffraction diagrams. We illustrate our formalism for X-ray scattering experiments performed on peapod samples synthesized from 2 different technics, which present different structural parameters. We propose and test different criteria to solve the difficult problem of the filling rate determination.

PACS. 61.46.+w Nanoscale materials: clusters, nanoparticles, nanotubes, and nanocrystals – 61.10.Dp Theories of diffraction and scattering – 61.10.Nz X-ray diffraction

1 Introduction

Since their discovery in 1991 [1], carbon nanotubes have been the purpose of a large number of studies, dealing both with their mechanical and electronic properties. In particular, it has been shown that the intercalation of electron donors or acceptors [2–4] into single wall carbon nanotubes (SWNT) bundles could dramatically modify the electronic properties of these objects. Rather large molecules are expected to be inserted into the hollow core of a nanotube that has been shown to present very stable adsorption sites [5]. C_{60} is one of the molecules that have successfully been inserted into SWNT, and a lot of studies have recently been achieved on the so-called "peapods". Those systems consist of SWNT in which C_{60} fullerene molecules are inserted [6]. Their study stands within the fascinating field of systems in a confined geometry [7–10]. Peapods structural analysis can be performed on a small number of tubes (and even on a single tube), using transmission electron microscopy (TEM) [6,11] or electron diffraction [12,13], or on macroscopic assemblies, using Raman spectroscopy [11,14,15] or X-ray scattering [15–17].

Theoretical and experimental studies have already been published on the diffraction diagram of powder of SWNT bundles [18,19]. In particular, the importance of the distribution of tube diameter on the position of the (10) Bragg peak in the X-ray and neutron diffraction patterns was pointed out in reference [19,20]. The complete study of the influence of all structural parameters of the bundles was performed using a simple numerical model. It was shown that modeling is essential for a correct determination of the structural parameters for such inhomogeneous samples of fairly crystallized nano-objects. Intercalated SWNT bundles form even more complex nano-crystalline systems. The adsorption sites can be separated into 3 main locations: inside the tubes, on the outer surface of the bundles (including the so-called "grooves" [5]) and into the interstitial channels of the 2D triangular lattice. Adsorption of a molecule into a SWNT bundle can involve modifications of the 2D triangular lattice (symmetry and/or lattice parameter expansion). These modifications lead to site-dependent diffraction diagram governed by the structure of the host (the nanotube bundle), the structure of the adsorbed species inside the bundles and by crossed interferences between the host and the molecules adsorbed. The modifications of the diagrams are also found to be radiation dependent [21]. Therefore, an efficient and correct interpretation of the diffraction diagram from such complex systems requires the use of simulation.

The study of the structure of C_{60} (and C_{70}) peapods by X-ray diffraction has recently been achieved by Kataura,

[a] e-mail: cambedou@gdpc.univ-montp2.fr

Maniwa and co-workers [15,16]. The authors could estimate the C_{60} (and C_{70}) filling rates from the analysis of their measurements. Also, the 1D lattice constant of the C_{60} chains inside the tubes was found to be smaller than those for 3D crystals of C_{60}. More strikingly, the temperature dependence of the corresponding feature in the diffraction diagram shows no dependence, indicating a nearly zero thermal expansion of the C_{60} chain inside the tubes, raising questions about possible polymerization of the C_{60} chains. X-ray diffraction is found to be a very powerful tool to probe the structure of C_{60} inside the tubes. However, further experimental work is needed to understand the properties of C_{60} peapods. Such experimental work should include diffraction investigations on samples showing peapods having various structural characteristics:

1. different tube diameters
2. different filling rates
3. bundles with various sizes e.g. various numbers of tubes

and particularly, to allow variable degrees of freedom for the fullerene molecules. Therefore, in this paper, we propose to give a detailed "step by step" and complete study of the diffraction patterns of peapods and we discuss the characteristic signatures linked to the insertion of C_{60} inside the SWNTs. We also show how the variation of different structural parameters, such as tube diameter, filling rate of SWNTs by C_{60}, and C_{60} adsorption in the outer groove sites at the surface of the bundles can change the shape of the diffraction pattern. The reader has to keep in mind that this report is an attempt to give experimentalists the necessary tools to characterize their samples by X-ray and/or neutron diffraction. Very often it appears that unexpected impurity phases are present in SWNT samples, as revealed by a comparison between X-ray and neutron diffraction patterns measured on the same powder. Therefore both techniques are complementary. In the first part of this paper, we present the theoretical model used to achieve the simulations. We consider a powder of uncorrelated tubes filled with C_{60} in the second part, and the third part deals with powder of bundles of peapods. Polymerization of the C_{60} chains is also considered. We finally compare the results of our calculations with experimental diffraction patterns. A large part of the discussion is concerned with the determination of the filling rate in the investigated samples. Let us also mention here, although it is beyond the scope of this article devoted to powder scattering, the interest of structural studies on partially aligned peapod samples [17], which can allow one to separate the nanotube and the C_{60} signals and can thus give supplementary information.

2 Principle of the calculations

In our attempt to reproduce the diffraction pattern of peapods, we developed a model based on the general equations for X-ray and neutron diffraction in the kinematical approximation [22,23] for which the diffracted intensity is proportional to the squared modulus of the scattering amplitude. The latter is defined as the Fourier transform of a configuration of atoms in the scattering volume. The diffracted intensity thus writes as follows:

$$I(\vec{Q}) \propto \left| \int_{volume} f_s \rho(\vec{r}) e^{i\vec{Q}\cdot\vec{r}} d^3\vec{r} \right|^2 \quad (1)$$

where $\vec{Q}$ is the scattering vector, $\rho(\vec{r})$ is the density of scatterer at position $\vec{r}$ in the sample, and f_s depends both on the scattering element (e.g. the atomic species) and on the nature of the incident radiation (f_s is a function of the wave-vector modulus Q for X-rays while it is constant for neutrons). Since we consider the case of a powder experiment, the diffraction is to be averaged over all the directions of space or, equivalently, over all the orientations of the scattering vector in the reciprocal space. The mean diffracted intensity is thus given by:

$$I(Q) = \frac{\int\int I(\vec{Q}) d^2 S(\vec{Q})}{4\pi Q^2} \quad (2)$$

where the integration is performed over the sphere of radius Q and $d^2S(\vec{Q})$ is a surface element of this sphere. Therefore, the model consists in choosing a convenient –and physically correct– mathematical form of the density of scatterer $\rho(\vec{r})$. A powerful approach consists in replacing the discrete carbon atoms by uniformly charged surfaces for both nanotubes and C_{60} molecules, with a surface atomic density $\sigma_c \sim 0.37$ atom/Å^2. This value is a little underestimated for C_{60} molecules (~ 0.39 atom/Å^2) but we take it as equal for the simplicity. This assumption results in a loss of information concerning the atomic arrangement at the surface of the objects forming the sample. It limits the reliability of our results to Q-values lower than 2 Å^{-1}. Below this value, the diffraction pattern is indeed insensitive to the detailed atomic order. It is however very much affected in this Q range by the medium range organization e.g. the 2D hexagonal nanotubes bundles and the 1D C_{60} packing. In the following, we will therefore be concerned with the two latter levels of organization in the framework of the homogenous approximation.

The detailed parameters of the model and the definition of the different variables used thorough this work are presented in Figure 1:

- The upper part represents a single tube filled with a linear chain of C_{60}s. Each C_{60}-filled nanotube will be considered as a linear superposition of 1D unit cell, each cell consisting of a cylinder of length L and of a single C_{60} molecule located at its center.
- The lower part represents the peapods organized into bundles e.g. on a 2D hexagonal lattice, the parameter of which is a function of the tubes diameter forming it. We introduced a random shift T_z between the position of the C_{60} molecules on one tube with respect to the corresponding position on the central tube to avoid unrealistic correlations between the positions of the C_{60}s inside the different nanotubes of the same bundle.

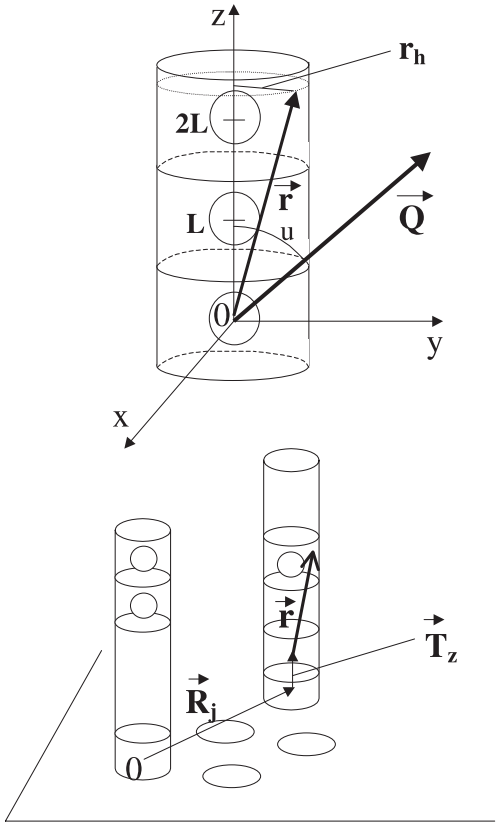

Fig. 1. Schematic representation of the system of coordinates and variables used in the calculations.

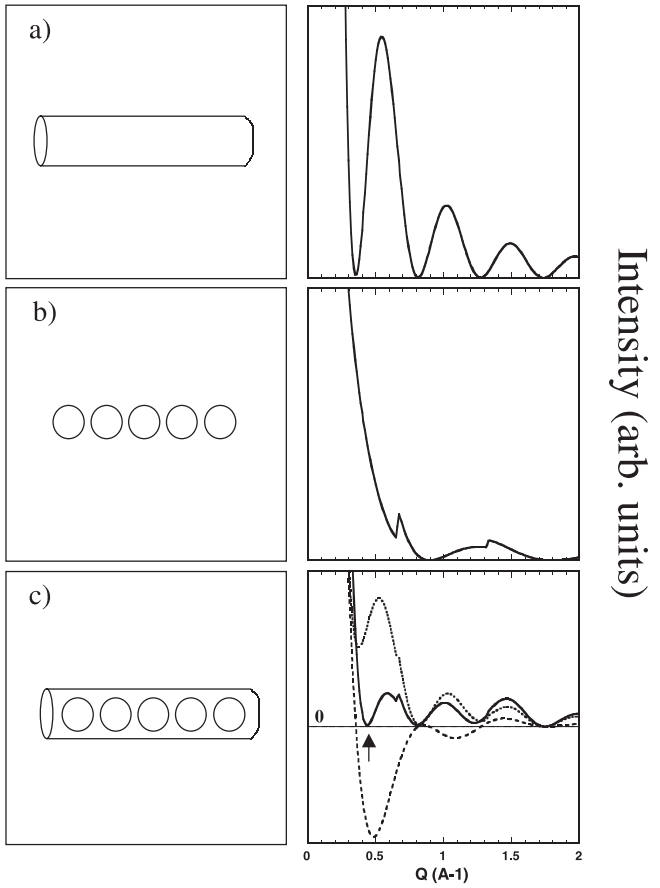

Fig. 2. Calculations of the intensity diffracted by several powders. a) nanotube of radius $r = 6.8$ Å and of length 380 Å. b) linear chain of 40 C_{60} molecules. c) peapod (plain line), sum of the intensities from a) and b) (dotted line), and crossed term (dashed line).

3 Isolated tubes filled with a chain of C_{60} molecules: isolated peapods

3.1 Complete filling of the nanotubes

In this part, we discuss the main features of the diffraction pattern calculated for a powder of 380 Å long and 13.6 Å large peapods that is obtained by stacking 40 cylinders of length 9.5 Å, each cylinder containing a 3.5 Å radius sphere at its center (see Fig. 1). This value of 9.5 Å is not deduced from measurements. It must be considered as a parameter of the model. We present in Figure 2 the calculated intensity for this object (bottom), for the tube alone (top) and for a C_{60} chain alone (middle).

Let I_t be the intensity diffracted by a powder of empty nanotubes. It is a pseudo-periodic oscillating function which is proportional to the squared modulus of the zero order cylindrical Bessel function J_0, as it appears in the following expression of I_t:

$$I_t(Q) \propto \int_{u=0}^{\pi} \left|A_t(\vec{Q})\right|^2 \sin(u)du \qquad (3)$$

with A_t the amplitude scattered by the empty nanotube:

$$A_t(\vec{Q}) = 2\pi L r_h f_s \sigma_c J_0\left(Q r_h \sin(u)\right) \frac{\sin\left(Q\frac{L}{2}\cos(u)\right)}{Q\frac{L}{2}\cos(u)} \times \sum_{n=0}^{40} e^{iQnL\cos(u)} \qquad (4)$$

and where u, L and r_h are defined in Figure 1 and where n labels the 1D unit cells (cylinders of length L).

Let I_c be the intensity diffracted by a powder of linear chains of C_{60} molecules:

$$I_c(Q) \propto \int_{u=0}^{\pi} \left|A_c(\vec{Q})\right|^2 \sin(u)du \qquad (5)$$

where A_c is the amplitude scattered by the linear chain of C_{60} molecules:

$$A_c(\vec{Q}) = 4\pi r_{C_{60}}^2 f_s \sigma_c \frac{\sin(Q r_{C_{60}})}{Q r_{C_{60}}} \sum_{n=0}^{40} e^{iQnL\cos(u)} \qquad (6)$$

and where $r_{C_{60}}$ is the radius of a C_{60} molecule (3.5 Å) [24]. This intensity is also a pseudo-periodic oscillating function, but with a pseudo-period that is nearly twice as long as the one of the nanotubes. Indeed, the radius of a C_{60} is nearly half the radial dimension of the tube. Another interesting feature of the latter curve is the asymmetric peak at 0.68 Å^{-1}, which results from the periodic positions of C_{60}s along the linear chain [25].

The first minimum of the intensity diffracted by the whole peapod (pointed by an arrow in Fig. 2) is located at $Q = 0.44$ Å^{-1}, whereas it was located at 0.38 Å^{-1} in the empty SWNT diffraction pattern. Following the work on gas adsorption inside SWNT by Maniwa et al. [26], Kataura et al. gave a simple explanation for this feature [15]: the reason for the presence of this minimum at this precise value of Q is due to the sum of the structure factors of the tube and of the C_{60} which equals zero for $Q = 0.44$ Å^{-1}. We will discuss this effect in slightly different term. Let us write the intensity $I_p(Q)$ diffracted by a peapod as follows:

$$I_p(Q) \propto \int\int \left| A_t(\vec{Q}) + A_c(\vec{Q}) \right|^2 d^2\vec{Q}. \quad (7)$$

According to the fact that A_t and A_c may be complex, relation (7) can be developed as:

$$I_p(Q) \propto I_t(Q) + I_c(Q) + 2\int\int \Big[\mathrm{Re}(A_t(\vec{Q}))\mathrm{Re}(A_c(\vec{Q})) + \mathrm{Im}(A_t(\vec{Q}))\mathrm{Im}(A_c(\vec{Q})) \Big] d^2\vec{Q} \quad (8)$$

where $\mathrm{Re}(A_t)$ and $\mathrm{Im}(A_t)$ stand for the real and imaginary parts of A_t, respectively. Relation (8) can be rewritten as:

$$I_p \propto I_t + I_c + I_{CI}. \quad (9)$$

If attention is given to Figure 2c, it is clear that the profile of I_p is quite different from $(I_t + I_c)$. This latter quantity is indeed the signature of a sample containing a tube decorrelated from a linear chain of C_{60}. In a peapod sample, there is a strong correlation in the relative positions of the tube and the chain of C_{60}, since the C_{60}s are located inside the tube. This correlation is revealed by the presence of the crossed interference term I_{CI} which can be positive or negative. At $Q = 0.44$ Å^{-1}, the crossed term compensates the $(I_t + I_c)$ term, lowering I_p to zero or nearly zero [27]. This value for Q is accidently the same as that of the (10) peak position for a bundle made of empty SWNTs stacked into a 2D hexagonal lattice. This coincidence will cause dramatic changes in the diffraction pattern relative to peapods bundles (see Sect. 4).

The increase of the tube diameter induces a decrease of the oscillation period as it is expected when considering larger diffracting object (see Fig. 3). The C_{60} periodicity characteristic peak at 0.68 Å^{-1}, as well as its first harmonic at 1.36 Å^{-1}, are observable in all the calculated diffraction profiles. For peapods of radius $r = 5.42$ Å (for example C_{60}@(8,8) peapods) the first peak is not separated from the first oscillation, but is clearly visible. The same behavior is observed for $r = 8.1$ Å peapods (for example C_{60}@(12,12) peapods) on the second oscillation, but the peak amplitude is weaker. In fact, the larger the tube diameter and the weaker this peak. The latter effect can be easily understood: an increase of the tube diameter implies an increase of the tube surface which leads to a preponderance of the response of the tubes over the response of the C_{60} chains, in which the number of scatterers remains unchanged. The cases of C_{60}@(8,8) and C_{60}@(12,12) peapods are discussed here as extreme cases for the influence of the tube diameter. However, it must be pointed out that the insertion of C_{60} in a (8,8) peapod is unlikely due to the too small diameter of the tube, and C_{60}s inside a (12,12) peapod would possibly lead to zigzag or helical chains in place of linear chains, since the center of the tube is no longer the most favorable location for C_{60} regarding to van der Waals interactions.

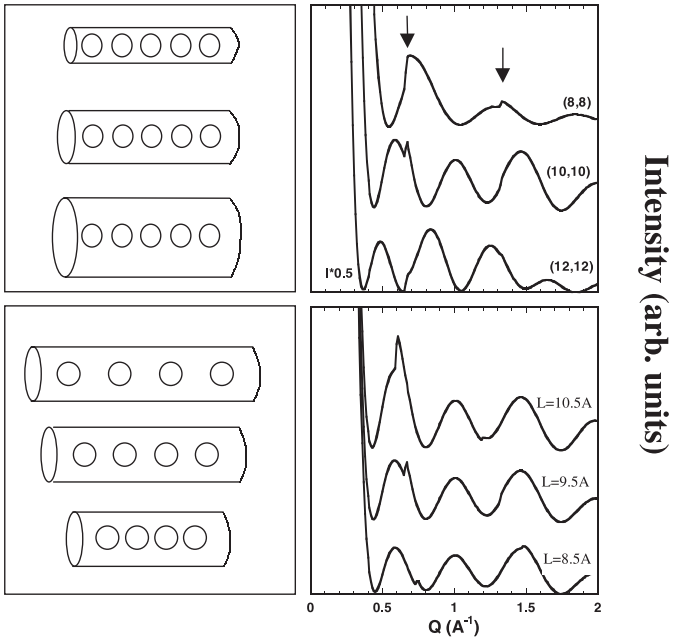

Fig. 3. Upper part of the figure: calculated powder diffraction patterns of peapods for different tube radii: 5.42 Å (8,8), 6.8 Å (10,10), 8.1 Å (12,12), with an inter-C_{60} distance L equal to 9.5 Å. Lower part of the figure: calculated diffraction patterns for different inter-C_{60} distances L and for a $r = 6.8$ Å tube.

The bottom part in Figure 3 reveals the consequences of a change in the inter-C_{60} length L inside the linear chain. A downshift of the characteristic peak of C_{60}s periodicity is evidently observed when L increases, but we also note a reinforcement of its intensity. One remarks a striking effect: although the relative density of C_{60} increases, the characteristic peak relative to the C_{60} periodicity strongly decreases. This is due to the multiplication factor arising from the intensity diffracted by a C_{60} molecule, which reaches its first zero at 0.9 Å^{-1}, as shown in Figure 2. The closer the peak position to this value, the weaker the peak. One must be careful with the fact that the respective proportion between tube and C_{60}s is no longer the pertinent parameter to account for the explanation of the changes in the peak intensities. Thus, it

may prove dangerous to focus only on the relative intensity of this peak, and it seems necessary to consider the whole diffraction pattern to derive reliable structural information.

In several cases, the use of an analytical formula can prove more comfortable than the method presented above. For infinite tubes, numerical calculations are performed after the limit of infinite tube length was taken in the above equations, leading to the following equation (demonstrated in Appendix A, Eq. (16)), where the first term comes from the Fourier transform of the structure projected in a plane perpendicular to the tube axis, while the second one comes from the periodicity of the C_{60} chains:

$$I_p(Q) \propto \frac{f_s^2}{Q}\left(\left(2\pi L r_h \sigma_c J_0(Q r_h) + 4\pi r_{C_{60}}^2 \sigma_c \frac{\sin(Q r_{C_{60}})}{Q r_{C_{60}}}\right)^2 + 2\mathrm{Int}\left(\frac{QL}{2\pi}\right)\left(4\pi r_{C_{60}}^2 \sigma_c \frac{\sin(Q r_{C_{60}})}{Q r_{C_{60}}}\right)^2\right). \quad (10)$$

In this expression $\mathrm{Int}(\frac{QL}{2\pi})$ is the integer part of $(\frac{QL}{2\pi})$.

3.2 Partial filling of the nanotubes

In the case of a real sample, it seems reasonable to consider that all tubes may not be fully filled with C_{60}s, despite efforts made to obtain filling rates as high as possible [11]. Two different hypotheses are discussed here.

The first hypothesis is to consider a random filling of the tubes without assuming clustering effects inside the tubes: the molecules are randomly positioned within a tube, the only constraint being a minimum distance of L between them (one may note that it implies that in the limiting case of 100% filling, the molecules necessarily form ordered chains). Calculations are performed within the finite tube length model, for a given filling ratio of the nanotubes. The effects of a random incomplete filling of the nanotubes are presented in the upper part of Figure 4. One observes the vanishing of the C_{60}-C_{60} characteristic peak with decreasing filling rates; it completely disappears for filling rates below 85%. If we compare the shapes of the 85% and the 100% diffraction profiles, one finds that the minimum at 0.44 Å^{-1} for the 85% filled sample no longer lowers to zero. The additional intensity can be attributed to the effect of the disorder induced by the random filling of the nanotubes by the C_{60} molecules. Moreover, the first minimum in intensity shifts to lower Q values for decreasing rate of fullerenes, which can be explained as in Figure 2 by compensation effects between tube, fullerene and interference terms.

As a second hypothesis, one can consider the partial filling of the tubes with long ('quasi-infinite') chains of C_{60}. We assume here that the molecules tend to cluster within nanotubes. Indeed, this should correspond to a low energy configuration of the system, the energy being lowered by the attractive C_{60}-C_{60} interactions. This hypothesis is supported by observations reported in reference [13].

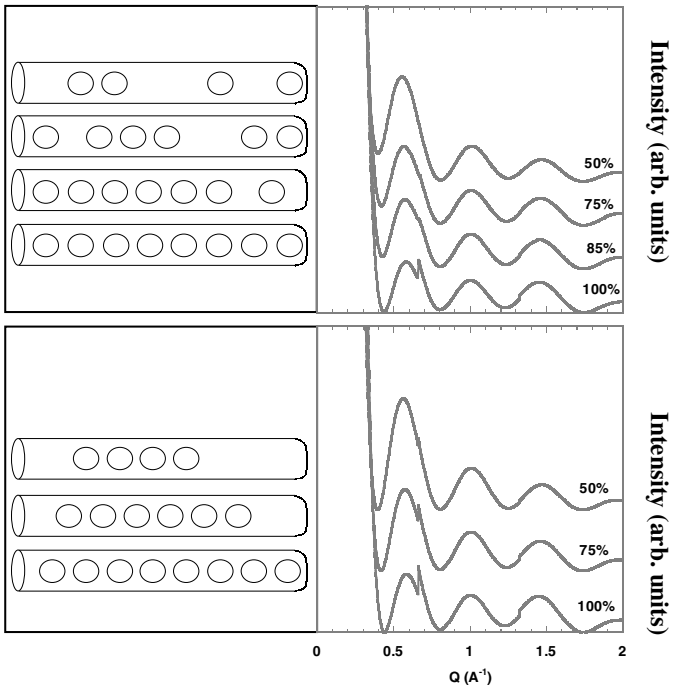

Fig. 4. Calculated diffracted intensities of a powder of isolated nanotubes (r_h = 6.8 Å). Up: for random filling by the C_{60} molecules (tube length is 380 Å); down: for incomplete filling by long ('infinite') C_{60} chains. Filling rates indicated in the figure are the same for all tubes in each case considered.

Calculated diffraction patterns for different filling rates (50%, 75% and 100%) are presented in the lower part of Figure 4. Here we use the infinite tube length model (detailed calculations are given in Appendix B). As it was already mentioned in the first hypothesis, we observe the vanishing of the C_{60}-C_{60} characteristic peak at low filling rates, but it interestingly disappears here for a filling rate of 50% which is much lower than the 85% observed in the first part. This is due to the long chains assumption: the C_{60}-C_{60} distance is preserved for the different filling rates. Another feature of these diffraction patterns is that the first minimum goes to zero for all filling rates, contrarily to what was found within the first hypothesis, which is due to lower disorder.

If one takes into account the differences pointed out between the 2 hypothesis discussed here, one should in principle be able to determine the way a sample of isolated peapods is filled. Unfortunately, the Q range around 0.44 Å^{-1} is usually perturbed by parasitic signals (intense scattering at small wave-vectors), so it is very difficult to use the value of the first minimum of intensity as a clue to determine the filling mode. As a result, the C_{60}-C_{60} characteristic peaks remain the only observable features for the estimation of the filling rate and of the filling mode. An important result from our calculations is that C_{60} molecules in isolated peapods with a random filling rate below 85% and peapods with a long chain filling rate under 50% are undetectable by diffraction.

3.3 Polymerized C_{60} molecules inside nanotubes

One of the remarkable properties of the C_{60} molecule is its ability to form covalent bonds through quite different routes. In crystalline C_{60}, polymers can be obtained (i) by photopolymerization, (ii) under pressure and at high temperature, (iii) in doped samples [28,29]. Photoinduced [11,15] and charge transfert induced [30] polymerization have also been demonstrated in C_{60} peapods, using Raman spectroscopy. It is interesting to consider the effect of polymerization on diffraction patterns. Let us consider peapods where the chains can be formed of n-polymers ($n = 1$: monomers, $n = 2$: dimers, $n = 3$: trimers...). For the sake of simplicity, we deal with the case of completely filled nanotubes. The distance L_b between bonded C_{60} molecules is taken to be 9.2 Å as in crystalline polymerized samples, and the distance L between unbonded molecules is fixed at 9.5 Å as above. The distance between monomers is smaller in peapods than in crystalline C_{60}, where it is equal to about 10 Å, possibly because of interactions with the nanotubes. However, there is no reason to take a smaller value for the distance between bonded molecules because it is mainly determined by the covalent bonding between them. It is shown in Appendix C that the scattered intensity of a powder of peapods filled with chains of n-polymers writes:

$$I_p(Q) \propto \frac{f_s^2}{Q}\Bigg(\Bigg(2\pi r_h(L+(n-1)L_b)\sigma_c J_0(Qr_h) + 4\pi r_{C_{60}}^2\sigma_c n\frac{\sin(Qr_{C_{60}})}{Qr_{C_{60}}}\Bigg)^2 + 2(1-\delta_{M,0})\sum_{k=1}^{M}\Bigg(4\pi r_{C_{60}}^2\sigma_c\frac{\sin(Qr_{C_{60}})}{Qr_{C_{60}}} \times\frac{\sin(k\pi nL_b/(L+(n-1)L_b))}{\sin(k\pi L_b/(L+(n-1)L_b))}\Bigg)^2\Bigg) \quad (11)$$

where the second term appears only for Q values such that M –the integer part of $(\frac{Q(L+(n-1)L_b)}{2\pi})$– is not zero. Calculated patterns for $n = 1$, 2 and 3 are drawn in Figure 5. At each $Q = k2\pi/(L+(n-1)L_b)$ value (with k integer), asymmetric peaks characteristic of the chain periodicity can be observed. Despite the change of the period –equal to $(L+(n-1)L_b)$ – with n, the spectra look quite similar. It can easily be explained from equation (11): the asymmetric peak intensity is multiplied by $\left[\frac{\sin(k\pi nL_b/(L+(n-1)L_b))}{\sin(k\pi L_b/(L+(n-1)L_b))}\right]^2$, which is close to zero except for $k = n$, $2n$, ... The first intense peak of the n-polymer diffraction pattern is thus located at $Q = n2\pi/(L+(n-1)L_b)$: $Q = 0.672$ Å^{-1} for dimers, 0.676 Å^{-1} for trimers, to be compared with 0.661 Å^{-1} for monomers. The upper value, corresponding to infinite polymers, is $Q = 2\pi/9.2 = 0.683$ Å^{-1}.

In summary, scattering analysis of polymerization of C_{60} molecules in peapods samples should be based on a careful study of the position Q_0 of the first intense asymmetric peak, and on the search for lower intensity peaks at kQ_0/n ($n = 2, 3...; k = 1$ to $(n-1)$) to identify n-polymers.

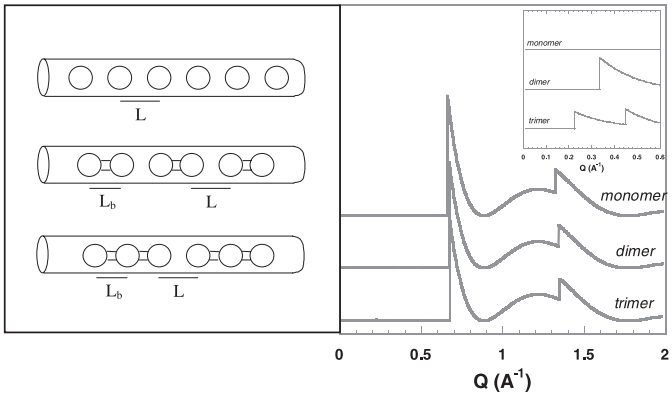

Fig. 5. Component of the calculated diffracted intensities relative to periodicity effects (only the second term of equation (11) is drawn) of a powder of isolated nanotubes ($r_h = 6.8$ Å), for C_{60} monomers (upper line), dimers (middle line) and trimers (lower line) chains inside the tubes.

4 Bundles of peapods

4.1 Complete filling

Peapods are packed into bundles where they are maintained together by van der Waals inter-tubes interactions. This organization is clearly visible on TEM pictures [11,15,16]. In this part, we calculate and discuss the diffraction pattern for such objects. Calculations are performed both for peapods of finite length and for peapods of infinite length (as detailed in Appendices A and B). The relative positions of the C_{60} chains along the tube axes (T_z in Fig. 1) are assumed to present no correlation from one tube to another. Indeed, a C_{60} chain interacts the most with the nanotube in which it is located, and nanotubes within a bundle present different helicities [31].

Figure 6 shows the comparison between the diffraction profiles calculated for a powder of bundles of 12 empty nanotubes and that of bundles of 12 peapods, with different tube radii. In all cases, we consider 380 Å long nanotubes organized on a 2D hexagonal lattice with a 3.2 Å van der Waals length between 2 adjacent nanotubes. Let us first consider the upper part of Figure 6, which deals with (10,10) tubes and peapods, of radius $r = 6.8$ Å. For peapods, the additional peaks characteristic of the 1D periodicity of the C_{60} chains are indicated by an arrow. We remark that most of the characteristic peaks observed in the diffraction pattern of the empty SWNT bundles show up in the diffraction pattern of the peapod bundles, except those located in the low Q range where a lack of intensity is obtained for the peapods. An important difference between the pattern of the peapod bundles and the empty nanotube bundles is thus the disappearance of the (10) Bragg peak at 0.44 Å^{-1}. This peak (of finite

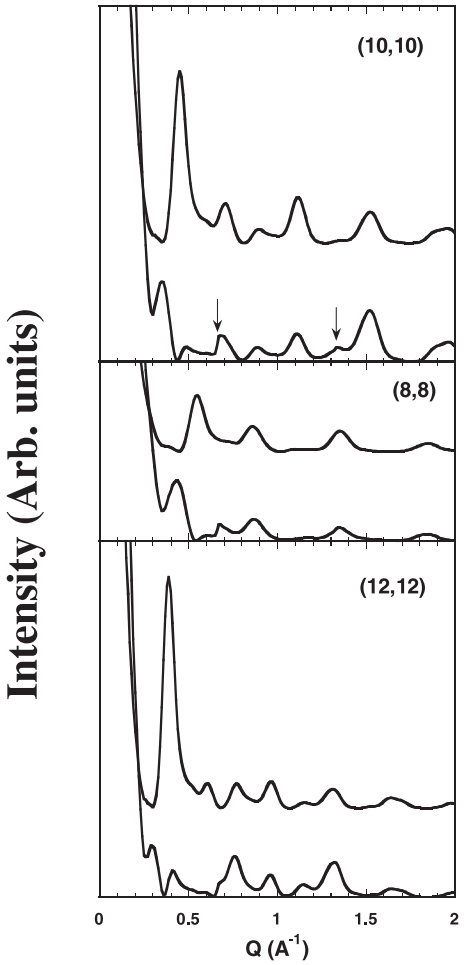

Fig. 6. Comparison between the calculated intensities scattered by a powder of bundles of 12 empty nanotubes (upper curve of each part) and bundles of 12 peapods (lower curve of each part) for (10,10) nanotubes (upper part) of radius $r = 6.8$ Å, (8,8) nanotubes (middle part) of radius $r = 5.42$ Å and (12,12) nanotubes (lower part) of radius $r = 8.1$ Å. The tube length was fixed at 380 Å in all the calculations. The arrows in the upper part point toward assymetric peaks characteristic of the 1D periodicity of C_{60} chains.

width because of the small bundle size) is replaced by a minimum delimited by two smaller peaks. This can be explained on the basis of Section 3 results, since we observed that the intensity diffracted by a single peapod lowers to zero at 0.44 $Å^{-1}$, which is around the position of the (10) lattice peak of the bundles. This important extinction process in the case of SWNT bundles has already been found and discussed for different kinds of intercalated molecules like gas molecules [15,32] or in iodine doped nanotubes samples [21]. Middle and lower parts of Figure 6 show that the extinction phenomenon is modified when the tube diameter is changed. For example, we consider the case of bundles of 12 empty nanotubes and 12 peapods of radius $r = 5.42$ Å ((8,8) tubes, middle part of Fig. 6) and $r = 8.1$ Å ((12,12) tubes, lower part of Fig. 6). One can see that the (10) peak is not split into two parts for the bundle of (8,8) peapods, but appears shifted to lower Q values. By contrast, this peak completely disappears in the case of the bundle of (12,12) peapods. When tube is thinner or larger in diameter, the progressive loss of the accidental adequate conditions implies the extinction phenomenon to be lost.

It is important to be aware that the extinction can occur for values of Q that are slightly different from the (10) peak position. In that case the (10) peak does not appear split, but seems shifted because only one side of the peak is lowered. Therefore, a direct interpretation of such apparent shift in terms of a change of the lattice parameter is inappropriate, and direct conclusions about structural changes based on the observation of the (10) peak alone, prove very hazardous. The analysis of peapods diffraction patterns is consequently not straightforward and should be based on comparison between measurements and calculations.

4.2 Partial filling

As for isolated tubes, all tubes may not be fully filled with C_{60}s. In this section, 4 different filling modes are discussed.

The first case (case a) consists in a random filling, where each tube of the bundle is filled as described in Section 3.2. Calculations are performed within the finite tube length model. In the 3 other cases, which are treated within the infinite tube assumption (detailed calculations are given in Appendix B), the C_{60}s are all stacked into long chains, but the way these chains are distributed into the bundles changes with the case. One can indeed consider an homogeneous filling (case b), where the tubes are all filled with the same number of C_{60} molecules, or an inhomogeneous filling (case c), where the filling rate of each tube of the bundle is slightly different. The last case to be discussed (case d) consists in a mix of fully filled bundles and empty bundles (see the right part of Fig. 7).

We present the results for filling rates of 85% and 50% for bundles of 12 nanotubes of radius $r = 6.8$ Å in the left part of Figure 7. The main difference between all diffraction patterns calculated for a 85% filling rate and all those calculated for a 50% filling rate is visible in the low Q range. The (10) Bragg peak is indeed still splitted and almost invisible at the 85% filling rate, while it clearly reappears at the 50% filling rate. This observation can be explained by the fact that the accidental conditions allowing the extinction of the (10) Bragg peak are progressively lost when the proportion of C_{60} decreases in the sample.

If more attention is given to the a), b), c) and d) diffraction profiles for a given filling rate, other features linked to the different filling modes can be extracted from the figure. One can first consider the Q range below 0.6 $Å^{-1}$. The intensity in this region is the least for the b) configuration, which is the least disordered configuration. If we compare with the inhomogeneous filling (mode c), and then with the random filling (mode a), we observe a progressive increase of the intensity in the low Q range, corresponding to the progressive increase of the disorder

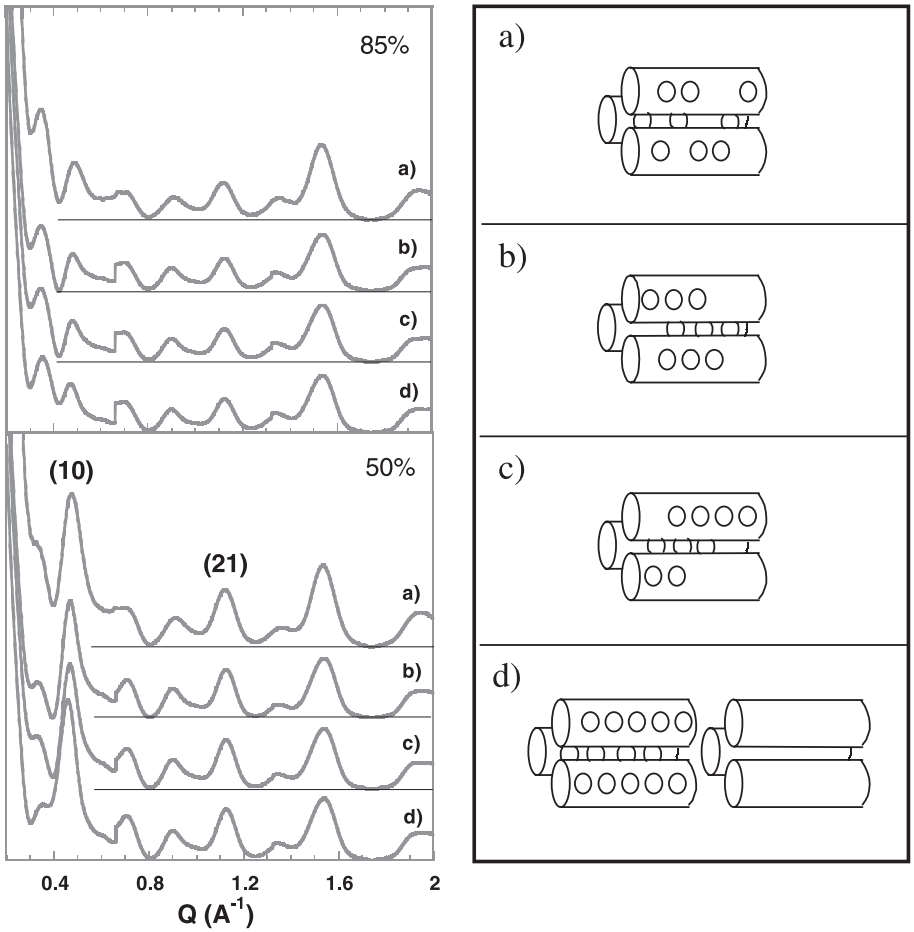

Fig. 7. Left top: Diffraction patterns of 85% filled bundles of 12 peapods. Left bottom: Diffraction patterns of 50% filled bundles of 12 peapods. All tubes have a radius of 6.8 Å. Right part: Schematic representations of the 4 different filling modes used in calculations: a) random positions for the C_{60} molecules within each tube, same filling for each tube, b) long C_{60} chains, same filling for each tube, c) long C_{60} chains, inhomogeneous filling of the different tubes within a bundle, d) mix of full and empty bundles.

in the system, as already mentionned in Section 3.2. The d) case must be considered separately from the other cases because the intensity in the low Q range is here the sum of the intensities of 2 decorrelated systems (full peapods and empty nanotubes).

One can also focus on the C_{60}-C_{60} characteristic peak. This asymmetric peak is clearly visible on the diffraction profiles of the b), c) and d) filling modes, even for the 50% filling rate, whereas it never appears at this rate for isolated peapods. In addition, this peak is invisible at both filling rates in the a) filling mode. Thus, the observation of such a feature in an experimental diffraction pattern should stand as the signature of a long chain organization of the C_{60} molecules inside the tubes.

4.3 Chains of C_{60} molecules in the outer groove sites of the bundles

We finally discuss the effects induced by the filling of the channels located at the bundle surface with linear chains of C_{60}s, for bundles of various size (Fig. 8). All tubes have a radius of 6.8 Å. When we consider the diffraction pattern of a 6 peapods bundle where the external channels have been completely filled, we note 2 main differences with regards to a naked peapod bundle. First, the peak at 0.68 $Å^{-1}$ is significantly reinforced due to the additional C_{60} molecules in the external channels. Secondly, the intensity in the low Q range as well as between 1 and 1.5 $Å^{-1}$ appears strengthened. As it is shown in Figure 2, the C_{60} response is high in these Q ranges, so this effect is just due to the increase of the C_{60} proportion in the sample. It is evidently clear that the higher the number of tubes in the bundle, the weaker the effect described just above. The reason for that lies in the simple fact that volume grows faster than surface when the size of the bundle increases. According to these results, we are able to conclude that an experimental diffraction pattern with a high intensity in the 1 to 1.5 $Å^{-1}$ Q range may be relative to a sample made of small sized bundles, saturated with C_{60}s in both the inner space of the tubes and in the external channels.

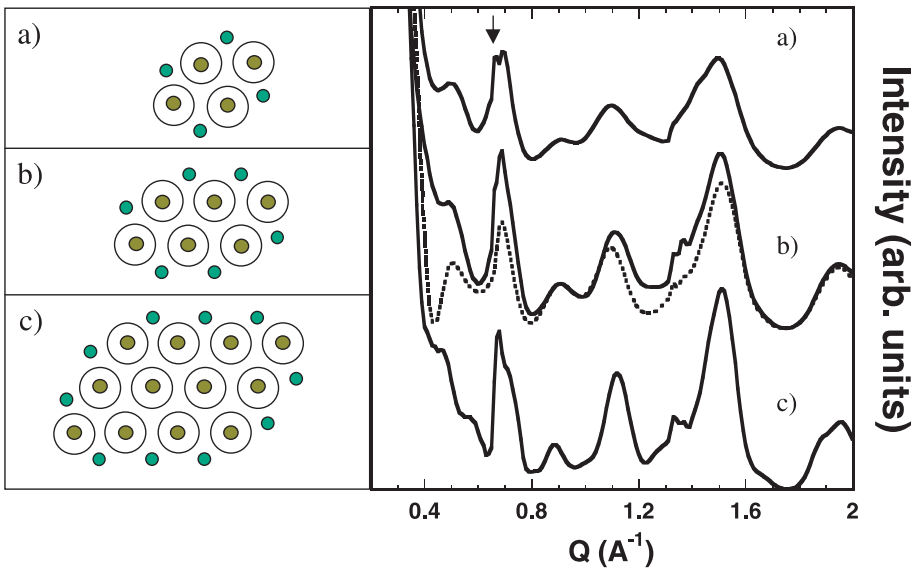

Fig. 8. Effect on diffraction pattern of the filling of the external channels with C_{60}s linear chains for different sizes of bundles. All tubes have a radius of 6.8 Å and are 380 Å long. a) 4 tubes. b) 6 tubes compared with a 6 tubes naked bundle (dotted line). c) 12 tubes.

4.4 Determination of the filling rate

In this section we try to define a method to determine the filling rate from experimental data. Two criteria are proposed which are based on the analysis of the results obtained from the model. As it was explained previously, the (10) Q range is strongly perturbed, so this Q range is disregarded. The first criterion consists to remark that the peak centered around 0.7 $Å^{-1}$ contains two contributions (Fig. 7): i) the response of the C_{60} lattice at 0.663 $Å^{-1}$ and ii) the (20) reflection of the bundle lattice centered at 0.706 $Å^{-1}$. The ratio of the two respective amplitudes is expected to vary as a function of the filling rate. However two problems arise. The first one concerns the type of filling which is unknown. The second concerns the background determination. We assume that the background can be represented by a straight line between 0.6 $Å^{-1}$ and 0.8 $Å^{-1}$ as is shown in the inset of Figure 9a. In Figure 9a the amplitude ratio is drawn as a function of the filling rate and for the two extreme types of filling, i.e. random and homogeneous (a) and b) cases, respectively). Cases c) and d) have intermediate behaviors, so they are not presented in this figure. Thus for a given experimental amplitude ratio (on vertical axis) one gets a range for the filling rate.

The second criterion consists to use: i) the amplitude of the C_{60} 1-D lattice peak around 1.3 $Å^{-1}$ as this peak arises in a Q range where the C_{60} contribution is strong, and ii) the amplitude of the (21) reflection of the bundles around 1.1 $Å^{-1}$ as the C_{60} contribution is small in this Q range. The calculated diagrams of Figure 7 were analyzed with a 3 peaks model from which we extracted the two amplitudes (Fig. 9b). Again the background estimation has a large incidence on the results.

The second criterion seems to be more reliable as it presents a smaller dependence on the type of filling. It is of easier use. However it has been established for SWNT bundles corresponding to diameters occuring in the case of electric arc or laser synthesis, i.e. centered around 1.4 nm and with a small dispersion in diameter distribution (FWHM $\leq$ 2 Å). In the next section these criteria are applied to the estimation of the filling rate in two different samples.

5 Comparison between calculated and experimental diffraction patterns

Diffraction patterns were performed using a powder diffractometer equipped with a curved position sensitive detector INEL CPS120 allowing one to measure simultaneously a range of 2θ angles from 2 to 120°. A wavelength of 1.542 Å was used. We measured the diffraction pattern of two different peapod samples (powder sample or numerous small pieces of bucky paper in glass capillaries). Sample A (Fig. 10a) was synthesized as follows: the SWNT material was first soaked in concentrated nitric acid (HNO_3 65%) and sonicated for approximatively 30 min, then treated in boiling HNO_3 at 140–150 °C for 4 hours. After sedimentation of the acid treated SWNT material in distilled water, SWNTs were separated from the acidic supernatant by centrifugation. The acid treated material was washed several times with distilled water (several centrifuge-washing-decantation cycles) then washed twice with ethanol. Finally, the SWNT material was dried under low pressure during overnight. The dried acid treated and washed SWNTs were subsequently heated in air at 420–430 °C for 30–40 min. After oxidation, the material was mixed with an excess of C_{60} powder in a glass tube. The glass tube was sealed under high vacuum, then heated at temperatures 550–600 °C for 72 hours. After heating,

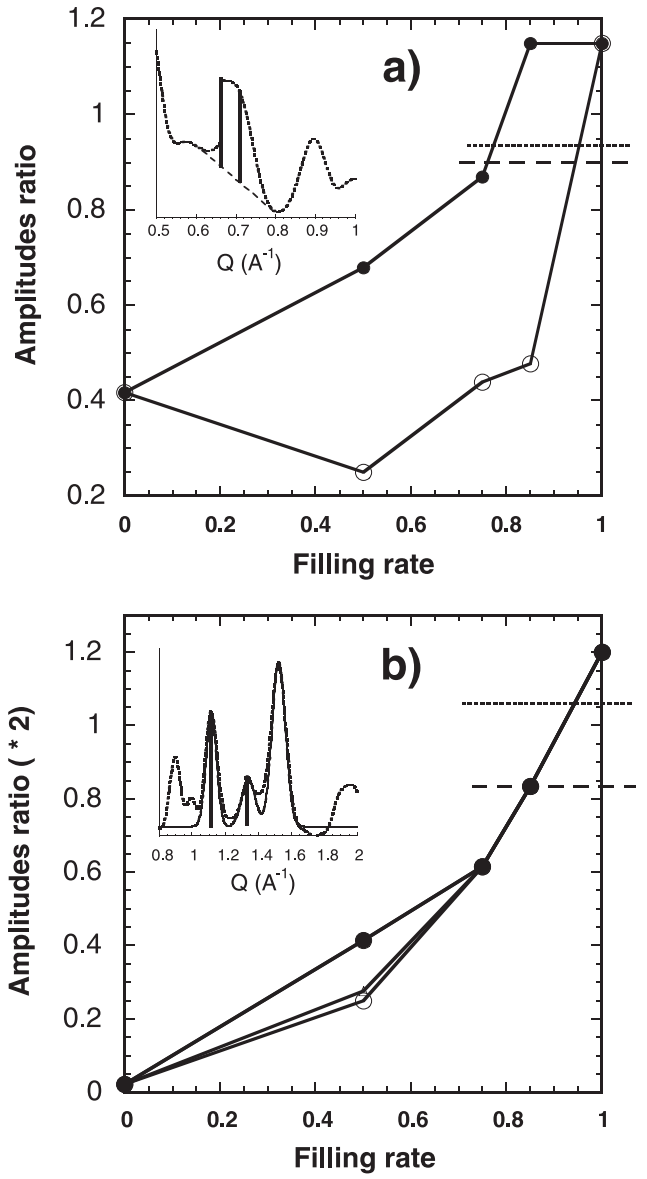

Fig. 9. Filling rate determination. a) First criterium giving the amplitude ratio $I(0.663\ \text{Å}^{-1})/I(0.706\ \text{Å}^{-1})$ as function of the filling rate p (see the inset), calculated for randomly filled (empty circles) and homogeneously filled (full circles) bundles of peapods. b) Second criterium: amplitude ratio of the peaks around 1.3 Å^{-1} and 1.1 Å^{-1} as function of p (see the inset), calculated for randomly filled (empty circles), inhomogeneously filled (empty triangles) and homogeneously filled (full circles) bundes of peapods. The dashed and dotted horizontal lines represent the experimental finding for the two investigated samples A and B.

the ampoule was cooled down to room temperature and opened. The excess of C_{60} was removed by washing the SWNT material with toluene. Finally, the material was washed once with ethanol and dried under reduced pressure for overnight. The preparation method of sample B (Fig. 10b) has been described previously [11].

The diffraction patterns of these two samples look quite different. We note the presence of a broad underlying structure from 1 to 2.2 Å^{-1} in the diffraction patterns of sample A (dotted line in Fig. 10a). Applying the two criteria defined in Section 4.4 to the determination of the filling rate (after substracting the dotted line for sample A), one obtains 75 to 95% (using the first method) compared to 85% (second method) for sample A, and 77 to 96% (first) compared to 95% (second) for sample B (see the horizontal lines in Fig. 9). However, as is shown below, if the criteria can be applied to sample B where characteristic C_{60} peaks are clearly observed, they only give an estimation of a upper value of the filling rate for sample A.

Diffraction profiles were fitted by optimized calculations. Calculated diffraction patterns were convoluted with a convenient resolution function in order to be compared with the experimental profiles. We also introduced a distribution of tube diameter in the calculation. The latter was considered to be of Gaussian shape [19,20].

Concerning sample A, the comparison with the pristine SWNT powder allows us to put forward the following main characteristics of the peapod diffraction profile: a weak (10) peak, an enlargement of the second peak at its low Q-side (0.68 Å^{-1}) and additional intensity around 1.3 Å^{-1}. We obtained the best fit of the diffraction pattern considering a structure made of small bundles of 6 peapods, with a large tube radius distribution centered around 6.8 Å and chains of C_{60}s in the external channels of the bundles. Considering the 4 filling modes described above, a very high filling rate implies a sharp peak at 0.68 Å^{-1}, standing for the C_{60}-C_{60} periodicity. Such a sharp peak is not observed in the diffraction pattern, so we introduced a distribution of C_{60}-C_{60} lengths from 9 to 10 Å into the model, leading to an improvement of the fit. This distribution could testify to the presence of mixed dimer, trimer or n-polymers chains of C_{60} into the tubes in this sample. However, if by-products of the chemical treatment were present inside nanotubes with the C_{60} molecules, this would explain the decrease of the (1,0) peak intensity together with an enlargement of the C_{60} periodicity peak since periodicity would be perturbated. We should thus note here that on the basis of the present results, the filling rate values determined here, above 75%, might be over-estimated.

Concerning sample B, the general shape of the diffraction profile is better fitted. Different kinds of filling modes have been studied in order to give a reasonable range for the filling rate. If a d) filling mode is chosen, we obtain the plain line of Figure 10b, and a filling rate of about 75%. The model includes 30 tubes per bundle with a very narrow distribution of tube radii centered at 6.76 Å (same radius as in Ref. [16]), and an inter-C_{60} length of 9.8 Å. The good agreement between the calculation and the rest of the diffraction pattern is the proof of a reliable characterization of the sample and of a high quality process of synthesis.

The diffraction patterns measured for both samples show up a clear difference in their respective structures. Clear features in the diffraction pattern of sample B allow an unambiguous characterization and a reliable estimation of its filling rate. Furthermore, our results are in

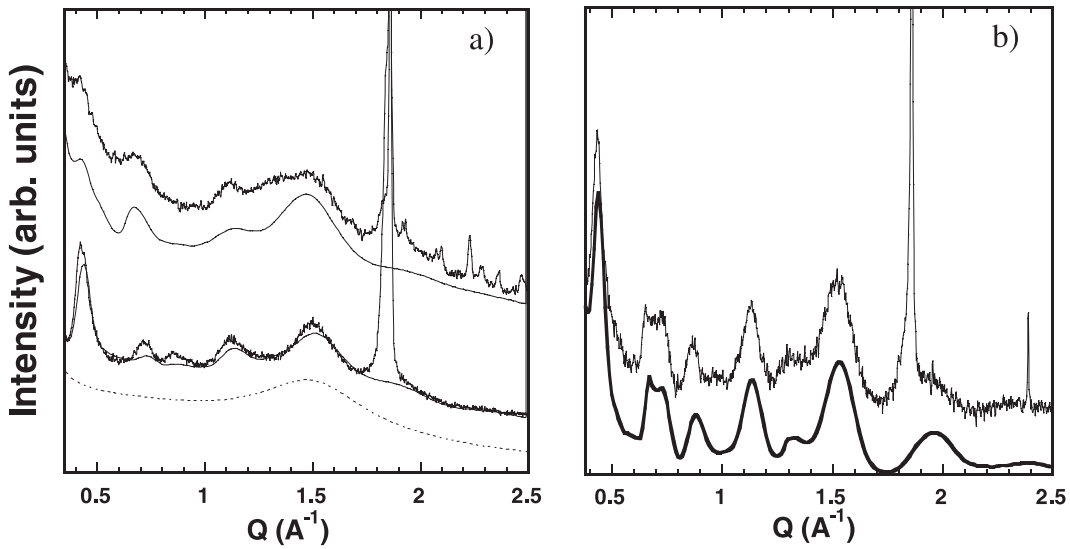

Fig. 10. Experimental diffraction patterns of peapod samples. a) Peapod sample A (upper line), corresponding MER pristine SWNT sample (lower line). The dotted line is the baseline used for the fits. b) Peapods sample B (upper line) and a calculation of its diffraction profile (lower line).

good agreement with what was previously determined for this sample in other X-ray diffraction and transmission electronic microscopy studies [15]. On the other hand, one must be more careful with the determination of the filling rate of sample A, as noted above.

6 Conclusion

We presented in detail the formalism to calculate the diffraction diagram of peapods at different level of organization: isolated and organized into bundles. This formalism allows to numerically investigate the main characteristics of the diffraction patterns of peapod samples, and to discuss those driving to a pertinent characterization of real samples. In particular, the isolated peapod study shows how the concentration of C_{60}s inside the tubes can shift the positions of the diffracted intensity zeros, and consequently lead to an accidental extinction of the (10) Bragg peak in the diffraction profile of peapod bundles, whereas there is no change in the bundle arrangement. These results show that one must be extremely careful about the correct interpretation of the changes in position and intensity of the (10) Bragg peak in experimental data concerning peapods and also all the inserted samples of SWNTs. Furthermore, we saw that the diffraction pattern of peapods has to be considered in its entire 0 to 2 Å^{-1} Q range in order to derive reliable characterization of the sample. In particular, much attention has to be paid to both the intensity and shape of the C_{60}-C_{60} characteristic peaks.

Those features are discussed in the measured diffraction patterns of two different samples.

It is our pleasure to acknowledge J.-L. Sauvajol and P.A. Albouy for fruitful discussions. H. Kataura acknowledges for a support by Industrial Technology Research Grant Program in '03 from New Energy and Industrial Technology Development Organization (NEDO) of Japan.

Appendix A

The calculation of the scattering pattern from a powder of peapods is detailed in this appendix for the case of nanotubes of infinite length.

For a given wavevector $\vec{Q}$ the intensity coming from an isolated peapod is:

$$I(\vec{Q}) = F(\vec{Q})F^*(\vec{Q}).$$

The form factor of a peapod of length L, containing one C_{60} molecule at half height, writes

$$F(\vec{Q}) = f_s\left(2\pi r_h L\sigma_c J_0(Q_{||}r_h)\frac{\sin(Q_zL/2)}{Q_zL/2} + 4\pi r_{C_{60}}^2\sigma_c\frac{\sin(Qr_{C_{60}})}{Qr_{C_{60}}}\right). \quad (12)$$

In this expression $\overrightarrow{Q_{||}}$ is the projection of the wavevector $\vec{Q}$ perpendicularly to the nanotube axis and Q_z is its projection along the axis.

For a peapod of length N_cL, it becomes

$$F(\vec{Q}) = f_s\left(2\pi r_h L\sigma_c J_0(Q_{||}r_h)\frac{\sin(Q_zL/2)}{Q_zL/2} + 4\pi r_{C_{60}}^2\sigma_c\frac{\sin(Qr_{C_{60}})}{Qr_{C_{60}}}\right)\sum_{n=0}^{N_c-1}\exp(iQ_znL). \quad (13)$$

The intensity per length unit thus writes

$$I(\vec{Q}) = f_s^2 \left[2\pi r_h L \sigma_c J_0(Q_{||} r_h) \frac{\sin(Q_z L/2)}{Q_z L/2} + 4\pi r_{C_{60}}^2 \sigma_c \frac{\sin(Q r_{C_{60}})}{Q r_{C_{60}}} \right]^2 \frac{1}{N_c L} \times \sum_{n=0}^{N_c-1} \exp(iQ_z nL) \sum_{m=0}^{N_c-1} \exp(-iQ_z mL). \quad (14)$$

Now we consider an infinite tube: $N_c \to \infty$. Using the relation

$$\lim_{N_c\to\infty} \frac{1}{N_c L} \sum_{n=0}^{N_c-1} \exp(iQ_z nL) \times \sum_{m=0}^{N_c-1} \exp(-iQ_z mL) = \frac{2\pi}{L^2} \sum_{k=-\infty}^{\infty} \delta(Q_z - 2\pi k/L)$$

where $\delta(x)$ is the Dirac distribution and where k is an integer, it follows that the intensity per unit length scattered by an isolated peapod of infinite length writes

$$I(\vec{Q}) = f_s^2 \left[2\pi r_h L \sigma_c J_0(Q_{||} r_h) \frac{\sin(Q_z L/2)}{Q_z L/2} + 4\pi r_{C_{60}}^2 \sigma_c \frac{\sin(Q r_{C_{60}})}{Q r_{C_{60}}} \right]^2 \frac{2\pi}{L^2} \sum_{k=-\infty}^{\infty} \delta(Q_z - 2\pi k/L)$$

which can be written as:

$$I(\vec{Q}) = f_s^2 \frac{2\pi}{L^2} \left[\left(2\pi r_h L \sigma_c J_0(Q_{||} r_h) \frac{\sin(Q_z L/2)}{Q_z L/2} + 4\pi r_{C_{60}}^2 \sigma_c \frac{\sin(Q r_{C_{60}})}{Q r_{C_{60}}} \right)^2 \delta(Q_z) + \left(4\pi r_{C_{60}}^2 \sigma_c \frac{\sin(Q r_{C_{60}})}{Q r_{C_{60}}} \right)^2 \sum_{k\neq 0} \delta(Q_z - 2\pi k/L) \right]. \quad (15)$$

The $\delta(Q_z)$ dependent term is the Fourier transform of the structure projected on a plane perpendicular to the nanotube axis, while the $\delta(Q_z - 2\pi k/L)$ dependent term comes from the periodicity of the C_{60} chain.

Now we use equation (2) to calculate powder average. If $g(Q_{||}, Q_z)$ represents the factor multiplicating $\delta(Q_z)$ in the previous expression, the integration of the $\delta(Q_z)$ dependent term over the angles u and φ gives

$$\int_0^{2\pi} d\varphi \int_{u=0}^{\pi} g(Q_{||}, Q_z) \delta(Q\cos(u)) \sin(u) du = \frac{2\pi}{Q} g(Q, 0)$$

where $Q_z = Q\cos(u)$. The integration of the $\delta(Q_z - 2\pi k/L)$ dependent term reduces to

$$\sum_{k\neq 0} \int_0^{2\pi} d\varphi \int_{u=0}^{\pi} \delta(Q\cos(u) - 2\pi k/L) \sin(u) du$$

which is equal to $[2\frac{2\pi}{Q}\mathrm{Int}(QL/2\pi)]$. Here $\mathrm{Int}(QL/2\pi)$ is the integer part of $(QL/2\pi)$: the asymmetric shape of the peaks characteristic of the C_{60} 1D periodicity can be understood through this formula (the sawtooth line shape).

It follows that the intensity scattered by a powder of *isolated* peapods is given by

$$I_p(Q) = \frac{(2\pi)^2 f_s^2}{QL^2} \left[\left(2\pi r_h L \sigma_c J_0(Q r_h) + 4\pi r_{C_{60}}^2 \sigma_c \frac{\sin(Q r_{C_{60}})}{Q r_{C_{60}}} \right)^2 + 2\mathrm{Int}(QL/2\pi) \left(4\pi r_{C_{60}}^2 \sigma_c \frac{\sin(Q r_{C_{60}})}{Q r_{C_{60}}} \right)^2 \right]. \quad (16)$$

Let us now calculate the intensity scattered by a powder of peapod *bundles*. The expression of the form factor of a bundle of peapods of length $N_c L$ is:

$$F(\vec{Q}) = f_s \sum_i \left[2\pi r_h L \sigma_c J_0(Q_{||} r_h) \frac{\sin(Q_z L/2)}{Q_z L/2} + 4\pi r_{C_{60}}^2 \sigma_c \frac{\sin(Q r_{C_{60}})}{Q r_{C_{60}}} \exp(iQ_z T_z(i)) \right] \times \exp(i\overrightarrow{Q_{||}}\overrightarrow{R_i}) \sum_{n=0}^{N_c-1} \exp(iQ_z nL) \quad (17)$$

where $\overrightarrow{R_i}$ is the tube i position and $T_z(i)$ is a random number between 0 and L (see Fig. 1). Using the above procedure, one finds that the intensity scattered by a powder of peapod *bundles* is given by

$$I_p(Q) = \frac{(2\pi)^2 f_s^2}{QL^2} \left[\left(2\pi r_h L \sigma_c J_0(Q r_h) + 4\pi r_{C_{60}}^2 \sigma_c \frac{\sin(Q r_{C_{60}})}{Q r_{C_{60}}} \right)^2 \sum_{i,j} J_0\left(Q R_{ij}\right) + 2N_T \mathrm{Int}(QL/2\pi) \left(4\pi r_{C_{60}}^2 \sigma_c \frac{\sin(Q r_{C_{60}})}{Q r_{C_{60}}} \right)^2 \right]. \quad (18)$$

The lattice term is $(\sum_{i,j} J_0\left(Q R_{ij}\right))$ where R_{ij} is the distance between tubes i and j ($R_{ij} = |\overrightarrow{R_i} - \overrightarrow{R_j}|$); N_T is the number of tubes per bundle. If one considers a distribution of tube diameters inside bundles, or distribution of bundle sizes, one can extrapolate the average procedures presented in reference [19].

Appendix B

This appendix details some intensity calculations in the case of a powder of nanotube bundles, for incomplete filling of the nanotubes by 'long' (quasi-infinite) chains of

fullerenes. The chains within each tube are assumed to be sufficiently long to allow one to describe their scattered intensity with Dirac distributions. This assumption implies that the formula derived below cannot be used for too small filling rates.

Giving the site (n) of a molecule in tube (i), we define the filling factor of the site (i,n) by a function $f(i,n)$ which is 1 if the site is occupied and zero otherwise. To calculate the intensity $I_p(Q)$ in the case of partial filling, one multiplies the C_{60} term in equation (17) in Appendix A by this filling factor.

One follows the orientational average procedure given in Appendix A but with $I(\vec{Q})$ replaced by its average over occupancies $f(i,n)$. One finds

$$I_p(Q) = \frac{(2\pi)^2 f_s^2}{QL^2} \left\{ \sum_{i,j} \left[(2\pi r_h L \sigma_c J_0(Qr_h))^2 + \langle p(i)p(j)\rangle \left(4\pi r_{C_{60}}^2 \sigma_c \frac{\sin(Qr_{C_{60}})}{Qr_{C_{60}}} \right)^2 + 2\langle p(i)\rangle (2\pi r_h L \sigma_c J_0(Qr_h)) \times \left(4\pi r_{C_{60}}^2 \sigma_c \frac{\sin(Qr_{C_{60}})}{Qr_{C_{60}}} \right) \right] J_0(QR_{ij}) + 2\sum_i \mathrm{Int}(QL/2\pi)\langle p(i)p(i)\rangle \left(4\pi r_{C_{60}}^2 \sigma_c \frac{\sin(Qr_{C_{60}})}{Qr_{C_{60}}} \right)^2 \right\}. \quad (19)$$

During the course of the calculation terms containing $\langle p(i)p(j)\rangle$ arise, where p(i) is the filling factor of tube i: $p(i) = \frac{1}{N_c(i)} \sum_{n=1}^{N_c(i)} f(i,n)$ where $N_c(i)$ is the number of C_{60} sites in tube i.

The filling rate of the sample, called $\langle p\rangle$ or p, is the double average of $f(i,n)$:

$$\langle p\rangle = \frac{1}{N_T N_c} \sum_{i=1}^{N_T} \sum_{n=1}^{N_c} f(i,n) \quad (20)$$

where the number of C_{60} sites has been taken to be the same for all tubes $N_c(i) = N_c$.

Three cases are considered.

(i) *Homogeneous partial filling of the tubes with long chains of C_{60}, all tubes having the same mean filling rate p, independent of i*: $p(i) = p$, independent of i.

In that case, equation (19) becomes:

$$I_p(Q) = \frac{(2\pi)^2 f_s^2}{QL^2} \left[\left(2\pi r_h L \sigma_c J_0(Qr_h) + p4\pi r_{C_{60}}^2 \sigma_c \frac{\sin(Qr_{C_{60}})}{Qr_{C_{60}}} \right)^2 \sum_{i,j} J_0(QR_{ij}) + 2N_T \mathrm{Int}(QL/2\pi) \left(p4\pi r_{C_{60}}^2 \sigma_c \frac{\sin(Qr_{C_{60}})}{Qr_{C_{60}}} \right)^2 \right]. \quad (21)$$

The C_{60} form factor $\left[4\pi r_{C_{60}}^2 \sigma_c \frac{\sin(Qr_{C_{60}})}{Qr_{C_{60}}} \right]$ is multiplied by the mean filling rate p. There is no other modification of equation (18) because one assumes that the C_{60} molecules agglomerate within nanotubes to form long chains.

(ii) *Partial filling of the tubes with long chains of C_{60} molecules, with filling rates different from one tube to another within each bundle.* In that case, one has to consider that

$\langle p(i)p(j)\rangle = \langle p^2\rangle$ if $i = j$

$\langle p(i)p(j)\rangle = \langle p\rangle^2$ if $i \neq j$ (no correlation from one tube to another). So that $\langle p^2\rangle - \langle p\rangle^2 \neq 0$.

For instance, one can consider within each bundle average proportions p of fully filled tubes and $(1-p)$ of empty tubes (which can be due to the fact that $p\%$ of the tubes are opened and $(1-p)\%$ are closed), which gives: $\langle p(i)\rangle = p$ and $\langle p(i)p(i)\rangle = p$, then $\langle p(i)^2\rangle - \langle p(i)\rangle^2 = p(1-p) \neq 0$.

The different fillings of nanotubes induce additional disorder in direct space, which corresponds to diffuse scattering in reciprocal space. The additional scattering is the most intense at small Q values as in the case of chemical disorder [22]. This approach is detailed in reference [33] for partial filling of zeolite channels with nanotubes. Equation (18) becomes

$$I_p(Q) = \frac{(2\pi)^2 f_s^2}{QL^2} \left[\left(2\pi r_h L \sigma_c J_0(Qr_h) + \langle p\rangle 4\pi r_{C_{60}}^2 \sigma_c \frac{\sin(Qr_{C_{60}})}{Qr_{C_{60}}} \right)^2 \sum_{i,j} J_0(QR_{ij}) + N_T \left(\langle p^2\rangle - \langle p\rangle^2 \right) \left(4\pi r_{C_{60}}^2 \sigma_c \frac{\sin(Qr_{C_{60}})}{Qr_{C_{60}}} \right)^2 + 2N_T \mathrm{Int}(QL/2\pi)\langle p^2\rangle \left(4\pi r_{C_{60}}^2 \sigma_c \frac{\sin(Qr_{C_{60}})}{Qr_{C_{60}}} \right)^2 \right]. \quad (22)$$

(iii) *Nanotubes in the same bundle are all filled or all empty, p% of the bundles corresponding to filled tubes and (1-p)% to empty ones.* The scattered intensity is the sum of the intensities for p fully filled bundles and for $(1-p)$ empty bundles. Equation (18) becomes:

$$I_p(Q) = p\frac{(2\pi)^2 f_s^2}{QL^2} \left[\left(2\pi r_h L \sigma_c J_0(Qr_h) + 4\pi r_{C_{60}}^2 \sigma_c \frac{\sin(Qr_{C_{60}})}{Qr_{C_{60}}} \right)^2 \sum_{i,j} J_0(QR_{ij}) + 2N_T \mathrm{Int}(QL/2\pi) \left(4\pi r_{C_{60}}^2 \sigma_c \frac{\sin(Qr_{C_{60}})}{Qr_{C_{60}}} \right)^2 \right] + (1-p)\frac{(2\pi)^2 f_s^2}{QL^2} \left[(2\pi r_h L \sigma_c J_0(Qr_h))^2 \sum_{i,j} J_0(QR_{ij}) \right]. \quad (23)$$

Appendix C

This appendix details calculations in the case of polymerized C_{60} molecules inside the tubes. The chains within the tubes are assumed to be formed of n-polymers of C_{60} molecules. The distance between bonded C_{60} molecules within a n-polymer is L_b, which is smaller than the distance L between C_{60} neighbors belonging to different n-polymers. For instance, for $n = 2$, one considers a chain of dimers and for $n = 3$ a chain of trimers.

The form factor of a n-polymer of C_{60} molecules writes

$$F_{n-polymer} = 4\pi r_{C_{60}}^2 \sigma_c \frac{\sin(Qr_{C_{60}})}{Qr_{C_{60}}} \left(\sum_{k=0}^{n-1} e^{iQ_z(k-\frac{(n-1)}{2})L_b} \right)$$

$$= 4\pi r_{C_{60}}^2 \sigma_c \frac{\sin(Qr_{C_{60}})}{Qr_{C_{60}}} \left(e^{-iQ_z\frac{(n-1)}{2}L_b} \frac{1-e^{iQ_z nL_b}}{1-e^{iQ_z L_b}} \right)$$

$$= 4\pi r_{C_{60}}^2 \sigma_c \frac{\sin(Qr_{C_{60}})}{Qr_{C_{60}}} \frac{\sin(Q_z\frac{nL_b}{2})}{\sin(Q_z\frac{L_b}{2})}$$

where $(k - \frac{(n-1)}{2})L_b$ is the position of the C_{60} molecule indexed by k within the n-polymer.

By replacing in equation (15) the monomer form factor by that of the n-polymer and the period L along the monomer chain by the one along the n-polymer chain, which is $(L + (n-1)L_b)$, one obtains:

$$I(\vec{Q}) \propto f_s^2 \Bigg[\Bigg(2\pi r_h (L + (n-1)L_b)\sigma_c J_0(Q_\parallel r_h) \times \frac{\sin(Q_z(L + (n-1)L_b)/2)}{Q_z(L + (n-1)L_b)/2} + 4\pi r_{C_{60}}^2 \sigma_c \frac{\sin(Qr_{C_{60}})}{Qr_{C_{60}}} \frac{\sin(Q_z\frac{nL_b}{2})}{\sin(Q_z\frac{L_b}{2})} \Bigg)^2 \delta(Q_z) + \left(4\pi r_{C_{60}}^2 \sigma_c \frac{\sin(Qr_{C_{60}})}{Qr_{C_{60}}} \frac{\sin\left(Q_z\frac{nL_b}{2}\right)}{\sin\left(Q_z\frac{L_b}{2}\right)} \right)^2 \times \sum_{k\neq 0} \delta(Q_z - 2\pi k/(L + (n-1)L_b)) \Bigg].$$

Powder average thus gives:

$$I_p(Q) \propto f_s^2 \Bigg[\frac{1}{Q} \Bigg(2\pi r_h (L + (n-1)L_b)\sigma_c J_0(Qr_h) + 4\pi r_{C_{60}}^2 \sigma_c n \frac{\sin(Qr_{C_{60}})}{Qr_{C_{60}}} \Bigg)^2 + \frac{2}{Q}(1-\delta_{M,0}) \sum_{k=1}^{M} \Bigg(4\pi r_{C_{60}}^2 \sigma_c \frac{\sin(Qr_{C_{60}})}{Qr_{C_{60}}} \times \frac{\sin(\pi k n L_b/(L + (n-1)L_b))}{\sin(\pi k L_b/(L + (n-1)L_b))} \Bigg)^2 \Bigg]$$

where M is the integer part of $(\frac{\mathbf{Q(L+(n-1)L_b)}}{\mathbf{2\pi}})$; the term $(1 - \delta_{M,0})$ was introduced to avoid the case $M = 0$.

References

1. S. Iijima, Nature **354**, 56 (1991)
2. R.S. Lee, H.J. Kim, J.E. Fischer, A. Thess, R.E. Smalley, Nature **388**, 255 (1997)
3. A.M. Rao, P.C. Eklund, S. Bandow, A. Thess, R.E. Smalley, Nature **388**, 257 (1997)
4. N. Bendiab, A. Righi, E. Anglaret, J.L Sauvajol, L. Duclaux, F. Beguin, Phys. Rev. B **63**, 153407 (2001)
5. M.R. Johnson, S. Rols, P.Wass, M. Muris, M. Bienfait, P. Zeppenfeld, N. Dupont-Pavlovsky, Chemical Physics **293**, 217 (2003)
6. B.W. Smith, M. Monthioux, D.E. Luzzi, Nature **396**, 323 (1998)
7. D.H. Kim, H.S. Sim, K.J. Chang, Phys. Rev. B **64**, 115409 (2001)
8. A. Rochefort, Phys. Rev. B **67**, 115401 (2003)
9. D.J. Hornbaker, S.J. Kahng, S. Misra, B.W. Smith, A.T. Johnson, E.J. Mele, D.E. Luzzi, A. Yazdani, Science **295**, 828 (2002)
10. J. Vavro, M.C. Llaguno, B.C. Satishkumar, D.E. Luzzi, J.E. Fischer, Appl. Phys. Lett. **80**, 1450 (2002)
11. H. Kataura, Y. Maniwa, T. Kodama, K. Kikuchi, H. Hirahara, K. Suenaga, S. Iijima, S. Suzuki, Y. Achiba, W. Krätschmer, Synthetic Metals **121**, 1195 (2001)
12. X. Liu, T. Pichler, M. Knupfer, M.S. Golden, J. Fink, H. Kataura, Y. Achiba, K. Hirahara, S. Iijima, Phys. Rev. B **65**, 045419 (2002)
13. K. Hirahara, S. Bandow, K. Suenaga, H. Kato, T. Okazaki, H. Shinohara, S. Iijima, Phys. Rev. B **64**, 115420 (2001)
14. H. Kuzmany, R. Pfeiffer, C. Kramberger, T. Pichler, X. Liu, M. Knupfer, J. Fink, H. Kataura, Y. Achiba, B.W. Smith, D.E. Luzzi, Appl. Phys. A **76**, 449 (2003)
15. H. Kataura, Y. Maniwa, M. Abe, A. Fujiwara, T. Kodama, K. Kikuchi, H. Imahori, Y. Misaki, S. Suzuki, Y. Achiba, Applied Physics A **74**, 349 (2002)
16. Y. Maniwa, H. Kataura, M. Abe, A. Fujiwara, R. Fujiwara, H. Kira, H. Tou, S. Suzuki, Y. Achiba, E. Nishibori, M. Takata, M. Sakata, H. Suematsu, J. Phys. Soc. Jpn **72**, 45 (2003)
17. W. Zhou, K.I. Winey, J.E. Fischer, T.V. Sreekumar, S. Kumar, H. Kataura, Appl. Phys. Lett. **84**, 2172 (2004)
18. A. Thess, R. Lee, P. Nikolaev, H. Dai, P. Petit, J. Robert, C. Xu, Y.H. Lee, S.G. Kim, D.T. Colbert, G.E. Scuseria, D. Tomanek, J.E. Fischer, R.E. Smalley, Science **273**, 483 (1996)
19. S. Rols, R. Almairac, L. Henrard, E. Anglaret, J.L. Sauvajol, Eur. Phys. J. B **10**, 263 (1999)
20. E. Anglaret, S. Rols, J.-L. Sauvajol, Phys. Rev. Lett. **81**, 4780 (1998)
21. N. Bendiab, R. Almairac, S. Rols, R. Aznar, J-L. Sauvajol, I. Mirebeau, Phys. Rev. B **69**, 195415 (2004)
22. A. Guinier, *X-ray Diffraction in Crystals, Imperfect Crystals and Amorphous Bodies* (Dover Publications, 1994)
23. S.W. Lovesey, *Theory of Neutron Scattering from Condensed Matter* (Oxford Science, 1984)

24. In the case of C_{70}-peapods, not detailed in this article, there can be different C_{70}-C_{70} distances depending on the molecule orientations [16]. The extension of the formalism presented here can be applied to C_{70} after modification of the basis equations (6) or (12). The subsequent powder average formulation becomes a little bit more complicated since the molecular form factor depends on the wave-vector and not only on its modulus
25. The maximum of the asymmetric peak originating from the C_{60} chains is situated at $Q = 2\pi/L = 0.66$ Å^{-1} for infinite chains. For finite chains, it becomes less abrupt and its maximum shifts to higher Q values (namely, 0.68 Å^{-1} for chains of 40 molecules in Fig. 3)
26. Y. Maniwa, Y. Kumazawa, Y. Saito, H. Tou, H. Kataura, H. Ishii, S. Suzuki, Y. Achiba, A. Fujiwara, H. Suematsu, Japanese J. Appl. Phys. **38**, L668 (1999)
27. The compensation leads to a zero value of the intensity for peapods of infinite lengths, and to values close to zero for finite lengths
28. B. Sundqvist, Adv. Phys. **48**, 1 (1999)
29. L. Forró, L. Mihály, Rep. Prog. Phys. **64**, 649 (2001)
30. T. Pichler, H. Kuzmany, H. Kataura, Y. Achiba, Phys. Rev. Lett. **87**, 267401 (2001)
31. L. Henrard, A. Loiseau, C. Journet, P. Bernier, Eur. Phys. J. B **13**, 661 (2000)
32. A. Fujiwara, K. Ishii, H. Suematsu, H. Kataura, Y. Maniwa, S. Suzuki, Y. Achiba, Chem. Phys. Lett. **336**, 205 (2001)
33. P. Launois, R. Moret, D. Le Bolloc'h, P.A. Albouy, Z.K. Tang, G. Li, J. Chen, Solid State Comm. **116**, 99 (2000)